


Article

# Prereduction of Nchwanging Ore in CO/CO<sub>2</sub>/H<sub>2</sub> Gas Mixtures

Trygve Lindahl Schanche \* and Merete Tangstad 

Department of Materials Science and Engineering, Norwegian University of Science and Technology, Alfred Getz vei 2, 7034 Trondheim, Norway; merete.tangstad@ntnu.no

\* Correspondence: trygve.l.schanche@ntnu.no

**Abstract:** Prereduction of Nchwanging manganese ore was investigated by isothermal reduction between 600 and 800 °C to optimize the conditions for industrial pretreatment of manganese ores. Experiments were conducted in CO/CO<sub>2</sub> gas mixtures with and without hydrogen at two different oxygen partial pressures. Ore in the size fraction 9.52–15 mm was reduced in a thermogravimetric furnace, and the O/Mn ratio from the chemical analysis was used to determine the extent of prereduction. The samples were investigated by X-ray diffraction to investigate the evolution of phases under the course of reduction. The X-ray diffraction revealed that bixbyite and braunite (I and II) were reduced to manganosite with no or limited formation of hausmannite. Reduction of iron oxides subsided with wüstite, which is stabilized by manganese in the monoxide phase, and hydrogen was seen to improve the reduction of iron oxides. Modeling revealed that the reduction rate increased 2.8-fold upon increasing the CO content from 30% to 70% in a CO/CO<sub>2</sub> gas mixture. The addition of hydrogen improved the reduction rate with factors of 1.3 and 2.6 for the low and the high oxygen partial pressures, respectively. Hence, the optimal conditions for pretreatment can be achieved by keeping the oxygen partial pressure as low as possible while adding hydrogen to the reducing gas and ensuring a high reduction temperature. Successful pretreatment limits the extent of the Boudouard reaction in the submerged arc furnace, reducing the amount of CO produced and, thus, reducing the CO available for pretreatment. Hydrogen is a useful addition to the pretreatment unit since it lowers the oxygen partial pressure and improves the kinetics of prereduction.

**Keywords:** prereduction; manganese production; kinetics; hydrogen; manganese ore



**Citation:** Schanche, T.L.; Tangstad, M. Prereduction of Nchwanging Ore in CO/CO<sub>2</sub>/H<sub>2</sub> Gas Mixtures. *Minerals* **2021**, *11*, 1097. <https://doi.org/10.3390/min11101097>

Academic Editors: Sunil Kumar Tripathy and Chenna Rao Borra

Received: 7 September 2021  
Accepted: 1 October 2021  
Published: 6 October 2021

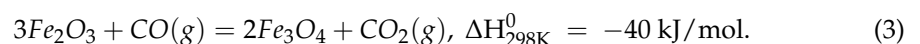
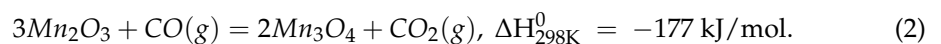
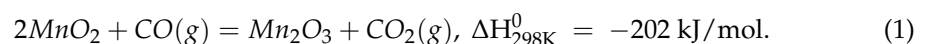
**Publisher's Note:** MDPI stays neutral with regard to jurisdictional claims in published maps and institutional affiliations.



**Copyright:** © 2021 by the authors. Licensee MDPI, Basel, Switzerland. This article is an open access article distributed under the terms and conditions of the Creative Commons Attribution (CC BY) license (<https://creativecommons.org/licenses/by/4.0/>).

## 1. Introduction

Manganese ferroalloys are mainly produced by carbothermic reduction in submerged arc furnaces (SAFs). Raw materials are added to the top of the furnace where the higher oxides of manganese and iron are reduced by the ascending CO gas from the metal production reaction in the lower parts of the furnace [1].



Most of the prereduction reactions are exothermic (reactions (1)–(5)); hence, the reduction will serve to preheat the charge mixture as it descends through the furnace. CO<sub>2</sub> is produced by the prereduction reactions and from carbonates in fluxes or ores. CO<sub>2</sub> produced at temperatures above 800 °C will react with solid carbon via the highly endothermic Boudouard reaction ( $C + CO_2(g) = 2CO(g)$ ,  $\Delta H_{298K}^0 = 172 \text{ kJ/mol}$ ), causing an excess consumption of carbon and energy [1]. This excess consumption can be avoided by improving the prereduction of the ore, where one option is to pretreat the ore prior to addition in

the furnace. Furnace off-gas constitutes an excellent heat and energy source and is available onsite. According to industrial measurements [2] and operating conditions [3], reductions in carbon consumption and energy consumption in the range of 303–455 kWh/ton metal and 76–114 kg C/ton metal can be achieved [4].

Industrial pretreatment of manganese ores has previously been conducted in rotary kilns. Ishitobi et al. utilized a rotary kiln for preheating and prereduction at 600–700 °C [5]. The rotary kiln was fueled by furnace off-gas, tire chips, coal, and kerosene [6]. Mass and energy balances were calculated for this unit by assessing the electrical energy consumption of the furnace. It was found that the electric energy consumption of the furnace was reduced by 25% if the pretreatment evaporated water, decomposed carbonates, and heated the raw materials to 600 °C [3]. Teguri et al. implemented a pretreatment operation to reduce and remove carbonates from the raw materials. Furnace off-gas (70% CO, 25% CO<sub>2</sub>, 5% H<sub>2</sub>) and coke were used as energy sources. Decarburization and prereduction to O/Mn = 1.19 (1 year average) was achieved with a 9 h residence time at 1150–1250 °C [7]. The addition of a pretreatment unit to the SAF will increase the raw material residence time in reducing conditions, lowering the amount of CO<sub>2</sub> evolved at temperatures above 800 °C [8] and, thus, reducing the energy and carbon consumption of the overall process. In addition, the removal of moisture and excessive oxygen improves furnace stability and safe operation [9,10].

Manganese ores have a wide range of chemical and mechanical properties; thus, they behave differently under reducing conditions. Several studies have been conducted investigating the reactivity of manganese raw materials non-isothermally, simulating the condition in the SAF. The excess oxygen, i.e., oxygen above MnO, present at 800 °C was used as a measure of reactivity. Higher excess oxygen content translates to lower reactivity since the excess oxygen will react with CO<sub>2</sub>, fueling the Boudouard reaction. From these studies, a positive correlation between porosity and reactivity was seen [2,11–14]. Changing the porosity of a raw material by sintering, briquetting, or pelletizing also changes the reactivity in a predictable manner [11,13,14]. The correlation between reactivity and porosity suggests that a lower mass transfer resistance in the material improves the reduction rate. Ngoy et al. found that addition of hydrogen to the reducing gas improved the reduction rate compared to CO–CO<sub>2</sub> mixtures with similar oxygen partial pressure [15]. Larssen et al. (2021) investigated the reduction of different size fractions of Nchwaning ore in various CO/CO<sub>2</sub> gas mixtures [16] and found that the reduction rate was proportional to the inverse average particle size and to p<sub>CO</sub> to the power of 1.5 [17]. The dependency on particle size is another indication that the reduction process is affected by diffusion resistance [18].

Pretreatment of the ore prior to the SAF shows potential in reducing energy consumption and carbon consumption and, in doing so, reducing CO<sub>2</sub> emissions in manganese ferroalloy production. If satisfactory prereduction can be accomplished at temperatures below 800 °C, the pretreatment unit may also accommodate the reductants and fluxes, giving the additional advantage of drying and preheating these materials. The off-gas from industrial furnaces has been reported to contain around 70% CO [7,19,20]; however, if pretreatment is successful, and the extent of the Boudouard reaction is reduced, the CO content of the off-gas will be reduced. Hydrogen can be produced from renewable sources and, thus, has the potential to be carbon-neutral. With its additional advantage of improving the reduction kinetics [15], it is an excellent candidate for pretreatment.

In this work, the reduction behavior of Nchwaning manganese ore was investigated in CO/CO<sub>2</sub> atmospheres with and without H<sub>2</sub>, aiming to determine the optimal conditions for pretreatment. While most of the previous work has been done using non-isothermal experiments to simulate the conditions in the SAF [2,11–14,16], this work determined the reactivity using isothermal experiments as the basis for designing a prereduction unit where hydrogen can also be used as a reductant.

## 2. Materials and Methods

Nchwaning ore was crushed and sieved, and the 9.52–15 mm fraction was selected for experiments. The material was split into representative samples of 150 g for the experiments, which were dried until constant weight at 105 °C to remove any surface moisture. The composition of the samples was determined by X-ray fluorescence (Bruker AXS S4 Pioneer X-Ray fluorescence spectrometer) using the fused bead technique. The excess oxygen was measured by titration (ASTM 465-11:2017), and the CO<sub>2</sub> content was measured by combustion IR (ELTRA). The result from analyzing three ore samples can be seen in Table 1. Excess oxygen was calculated from the titration results, yielding an O/Mn molar ratio of 1.5, implying an ore with manganese in a state similar to Mn<sub>2</sub>O<sub>3</sub>. The standard deviation of the chemical analyses was relatively high (Table 1), indicating heterogeneity in the ore. The amount of CO<sub>2</sub> in the sample indicates that some of the CaO (and/or MgO) was in the form of carbonate.

**Table 1.** Chemical composition (wt.%) of unreduced Nchwaning ore. Average and standard deviation (SD) (wt.%) based on three samples. The excess oxygen was calculated from the titration results and indicates the oxygen above MnO.

	Mn <sub>Tot</sub>	Fe	SiO <sub>2</sub>	Al <sub>2</sub> O <sub>3</sub>	CaO	MgO	CO <sub>2</sub>	O <sup>1</sup> <sub>excess</sub>
%	48.7	8.7	4.4	0.4	5.9	0.6	2.5	7.1
SD	3.3	2.5	0.2	0.1	0.6	0.3	0.5	0.4

<sup>1</sup> Calculated from the titration results.

The experiments were conducted in a thermogravimetric (TG) setup. The setup consisted of a vertical resistance furnace (Entech VTF 80/15), the position of which could be adjusted vertically to surround the crucible. The crucible was made of high-temperature stainless steel (steel grade 253 MA) and was suspended in a balance (Mettler Toledo PR2003DR) to record the weight changes continuously throughout the experiment. Figure 1 shows a sketch of the crucible. Multiple gases can be used, and there are separate mass flow controllers for each gas (Bronkhorst F-201C). The gases are mixed before entering the crucible and preheated as they pass through the double wall of the crucible before it reaches the sample (Figure 1). Ar, CO, CO<sub>2</sub>, and H<sub>2</sub> with purity of 99.999%, 99.97%, 99.9992%, and 99.9%, respectively, were used in the experiments. The sample weight was recorded on an external scale (Ohaus Pioneer PA4202) before and after the experiments to account for any drifting of the furnace balance.

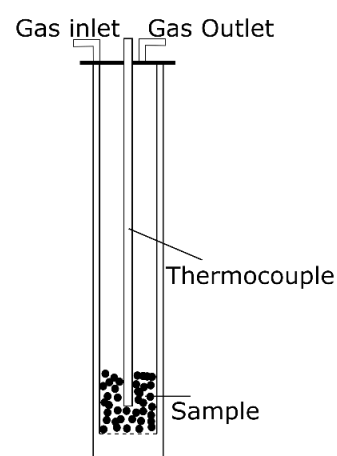


**Figure 1.** Sketch of the crucible used in the reduction experiments.

The samples were reduced at prescribed temperatures and gas mixtures, and a thermocouple was placed in the center of the material to measure the sample temperature. The furnace was heated to the prescribed temperature which was kept constant throughout the

experiment to achieve isothermal conditions at 600 °C, 700 °C, and 800 °C; however, the samples did not experience true isothermal temperature due to the exothermal reactions and heating time. The samples reached their highest temperature 15–35 min after the furnace was raised. This also means that some of the prereduction occurred before the sample reached the isothermal temperature. The reduction was conducted in mixtures of CO, CO<sub>2</sub>, and H<sub>2</sub>, and the composition of the different mixtures can be seen in Table 2. Cooling after the completion of an experiment was done in Ar.

**Table 2.** Composition of the gas mixtures used (vol.%).

CO	CO <sub>2</sub>	H <sub>2</sub>
30	70	0
70	30	0
16	68	16
37	26	37

The total flow rate of gas was 4 nL/min in all experiments. After reduction, one-quarter of the material was split from each sample and crushed. From the crushed material, samples were taken for chemical analysis (XRF) and X-ray diffraction (XRD). The XRD was done using a Bruker D8 A25 DaVinci X-ray Diffractometer with Cu-K $\alpha$  radiation and a LynxEye SuperSpeed detector scanning the range 15–75° with a 0.013° step size. Phases were indexed using the DIFFRAC.EVA V5.1 software coupled with the PDF-4+ database. Phase diagrams were calculated using the FToxid, FTmisc, and FactPS databases with Factsage [21], and the oxygen partial pressures in the gas mixtures were calculated using HSC chemistry 9 [22], allowing for O<sub>2</sub> and H<sub>2</sub>O in addition to the input gases.

XRD of the ore (Figure 2) revealed braunite (3(Mn,Fe)<sub>2</sub>O<sub>3</sub>·MnSiO<sub>3</sub>), braunite II (7(Mn,Fe)<sub>2</sub>O<sub>3</sub>·CaSiO<sub>3</sub>), and bixbyite ((Mn,Fe)<sub>2</sub>O<sub>3</sub>) as the major manganese-containing phases. These phases correspond to manganese in the Mn<sup>3+</sup> state (Mn<sub>2</sub>O<sub>3</sub>), which is consistent with the chemical analysis. Bixbyite, braunite, and braunite II have many overlapping peaks, as seen in Figure 2, but may be qualitatively distinguished on the basis of minor peaks [23]. Hematite (Fe<sub>2</sub>O<sub>3</sub>), manganite (MnOOH), hausmannite (Mn<sub>3</sub>O<sub>4</sub>), and calcite (CaCO<sub>3</sub>) were also identified in the diffraction pattern. The entry numbers and phases from the PDF-4+ database can be found in Table 3.

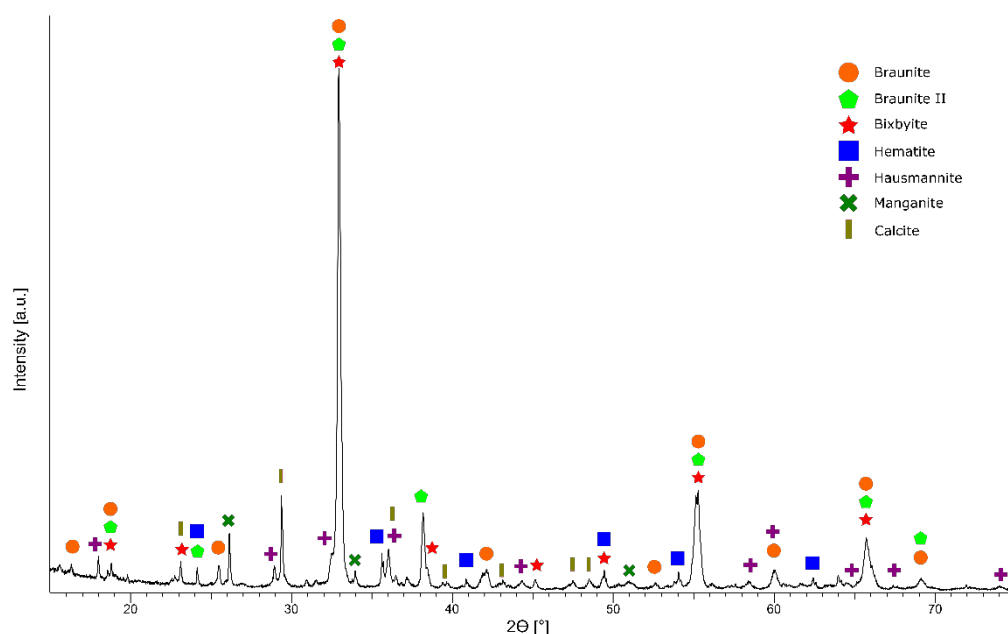


**Figure 2.** X-ray diffraction pattern of unreduced Nchwaning ore.

**Table 3.** Entry numbers and phases from the PDF-4+ database used to index diffraction patterns.

Utilized Indexing Patterns	
PDF 00-041-1367	Mn + 2Mn <sub>6</sub> + 3SiO <sub>12</sub> Braunite-1Q
PDF 04-007-2773	Mn <sub>0.74</sub> Fe <sub>1.26</sub> O <sub>3</sub> bixbyite, syn, manganese   Manganese Iron Oxide
PDF 00-041-1368	CaMn <sub>14</sub> + 3SiO <sub>24</sub> Braunite-2Q
PDF 00-033-0664	Fe <sub>2</sub> O <sub>3</sub> Hematite, syn
PDF 00-019-0629	Fe + 2Fe <sub>2</sub> + 3O <sub>4</sub> Magnetite, syn
PDF 00-041-1379	Mn + 3O(OH) Manganite
PDF 00-024-0734	Mn <sub>3</sub> O <sub>4</sub> Hausmannite, syn
PDF 01-075-6876	MnO Manganosite, syn
PDF 01-077-2362	(FeO) <sub>0.099</sub> (MnO) <sub>0.901</sub> ferrous manganese oxide   Iron Manganese Oxide
PDF 01-077-2361	(FeO) <sub>0.198</sub> (MnO) <sub>0.802</sub> ferrous manganese oxide   Iron Manganese Oxide
PDF 00-043-0697	(Ca,Mg)CO <sub>3</sub> Calcite, Mg-bearing
PDF 00-066-0867	Ca(CO <sub>3</sub> ) Calcite
PDF 04-007-9023	Mn <sub>2</sub> (SiO <sub>4</sub> ) Tephroite, syn

To investigate the repeatability and to get information regarding the intermediate reaction products, four experiments were conducted for each temperature in the CO/CO<sub>2</sub> gas mixtures. Two of the experiments were stopped at 30 and 90 min to investigate the phase evolution, and two experiments were run for 210 min, where complete reduction was achieved in 70% CO.

The effect of hydrogen on reduction was investigated using gas mixtures with  $p_{H_2} = p_{CO}$ . The thermodynamic characteristics of hydrogen as a reducing agent differ from those of CO. Table 4 shows the Gibbs free energy for reduction of Mn<sub>3</sub>O<sub>4</sub> at selected temperatures, and it can be seen that the thermodynamic driving force of reduction with H<sub>2</sub> and CO is equal at 815.5 °C. Reduction with H<sub>2</sub> has a higher driving force compared to CO at higher temperatures; conversely, reduction with CO has a higher driving force compared to H<sub>2</sub> at lower temperatures. To account for this difference, the CO<sub>2</sub> content of the H<sub>2</sub>-containing gas mixtures was decreased such that the thermodynamic driving forces, expressed by the partial pressure of oxygen, were similar to the CO/CO<sub>2</sub> gas mixtures used. The composition of the gases and oxygen partial pressures of the gas mixtures are shown in Figure 3. Experiments in CO/CO<sub>2</sub>/H<sub>2</sub> gas mixtures were run for 210 min with duplicates for each experiment. The experiment at 600 °C in 37% CO–26% CO<sub>2</sub>–37% H<sub>2</sub> was omitted due to soot formation.

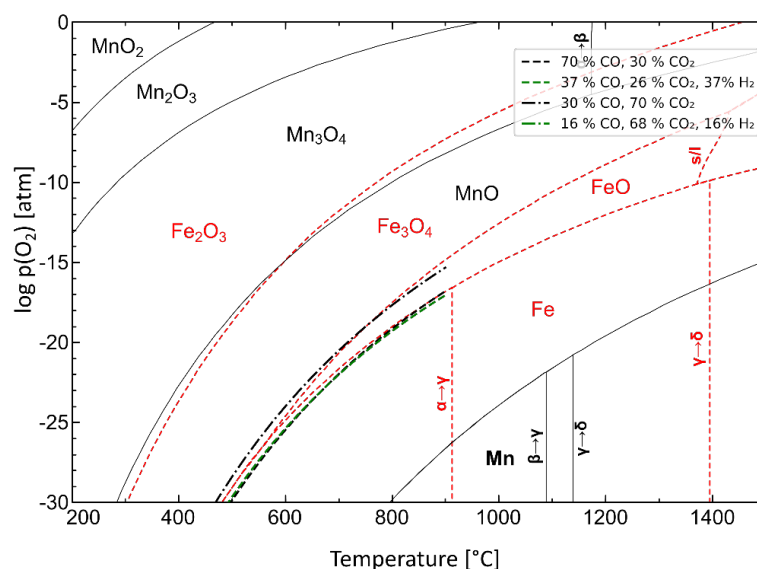


**Figure 3.** The oxygen partial pressure of the selected gas mixtures (green and black divided lines) superimposed on the Fe-O and Mn-O phase diagrams, showing oxygen partial pressure as a function of temperature.

**Table 4.** The Gibbs free energy for the reduction of  $Mn_3O_4$  by  $H_2$  and  $CO$  at selected temperatures [22].

Reaction	$\Delta G_{700\text{ }^\circ\text{C}}$	$\Delta G_{815.5\text{ }^\circ\text{C}}$	$\Delta G_{900\text{ }^\circ\text{C}}$
$Mn_3O_4 + CO(g) = 3MnO + CO_2(g)$	−81.6	−83.5	−85.6
$Mn_3O_4 + H_2(g) = 3MnO + H_2O(g)$	−76.9	−83.5	−88.2

When considering the iron content of the ore, the phase diagram in Figure 3 shows that magnetite ( $Fe_3O_4$ ) and wüstite ( $Fe_{(1-x)}O$ ) were stable at high  $pO_2$ , and metallic iron (Fe) was stable at low  $pO_2$ ; however, manganosite ( $MnO$ ) stabilized the iron as  $FeO$  in solid solution, as seen in the Mn–Fe–O phase diagram in Figure 4. Hence, the reduction was expected to subside with MnO–FeO. The reduction curves are presented as the O/Mn molar ratio as a function of time, where the recorded weight signal from the TG was calibrated to the initial and final O/Mn content on the basis of the chemical analysis.

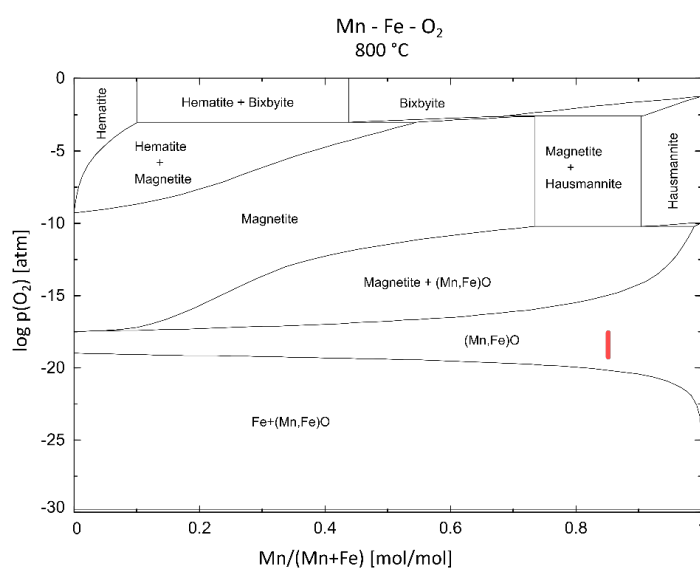


**Figure 4.** Phase diagram for the manganese–iron–oxygen system showing the stable phases as a function of oxygen partial pressure and composition at 800 °C. The experimental conditions are indicated by the red line.

### 3. Results and Discussion

The reduction curves for the different gas mixtures and temperatures can be seen in Figure 5. It can be seen that, within each gas mixture, the reduction rate and the extent of reduction increased with increasing temperature, which is consistent with previous investigations in this temperature range [17,24,25].

The rate and extent of reduction also increased with decreasing  $pO_2$  of the  $CO/CO_2$  gas mixtures (Figure 6). The oxides of manganese and iron display a wide range of solid solubility (Figure 4), and solid solutions between iron and manganese oxides have been seen to retard the reduction progress [16,26,27]. Larssen et al. investigated reduced and partly reduced Nchwaning ore and observed that the reduction of hematite subsided with the wüstite phase under conditions where the Fe–O phase diagram predicts metallic iron. This is explained by lowered activity of iron in the oxides, which is consistent with the SEM–EDS analysis of the ore, revealing a minor manganese content in the hematite (Fe/Mn molar ratio = 13.6) [16].



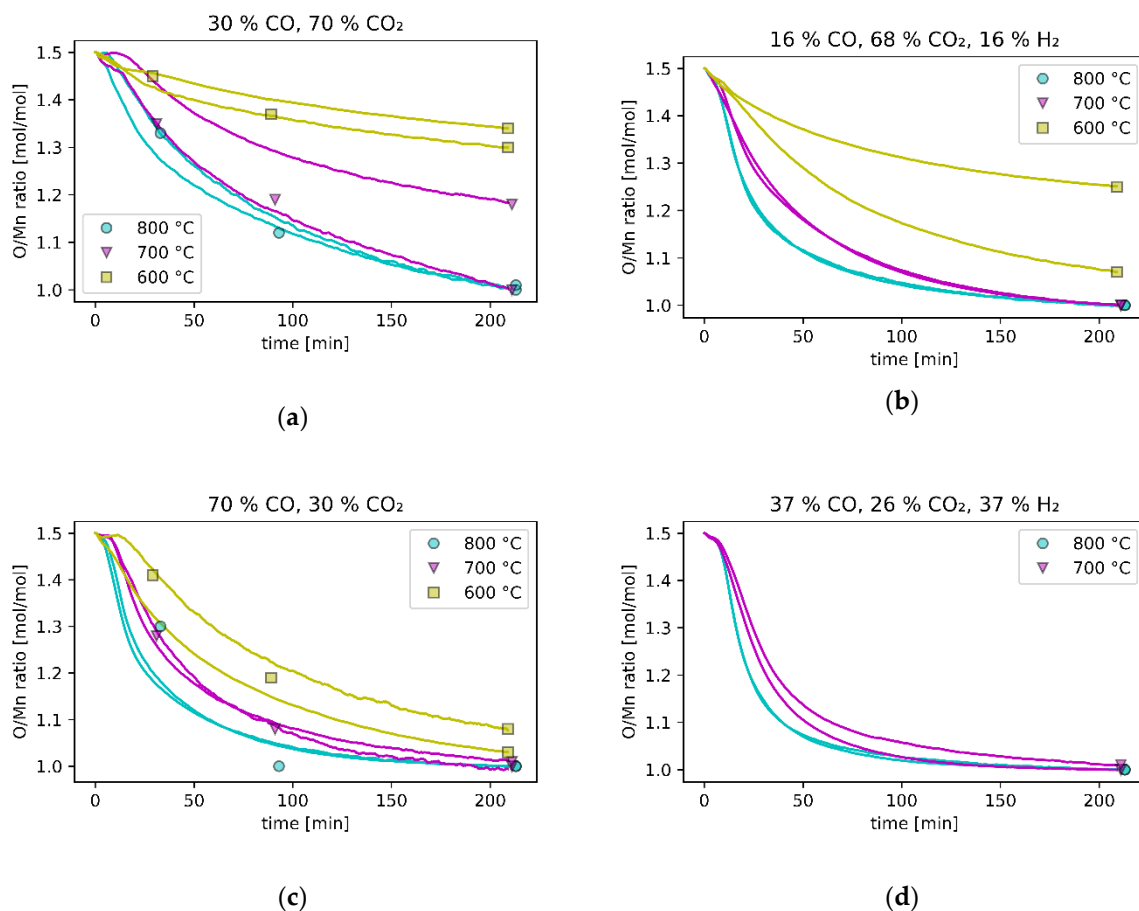


**Figure 5.** Reduction curves for the utilized gas mixtures. Markers indicate the analyzed *O/Mn* ratio from conducted experiments at 30, 90, and 210 min and are shifted slightly to avoid overlapping. Dashed lines show the results from modeling: (a): high  $p_{O_2}$  hydrogen-free experiments; (b): high  $p_{O_2}$  hydrogen-containing experiments; (c): low  $p_{O_2}$  hydrogen-free experiments; (d): low  $p_{O_2}$  hydrogen-containing experiments.

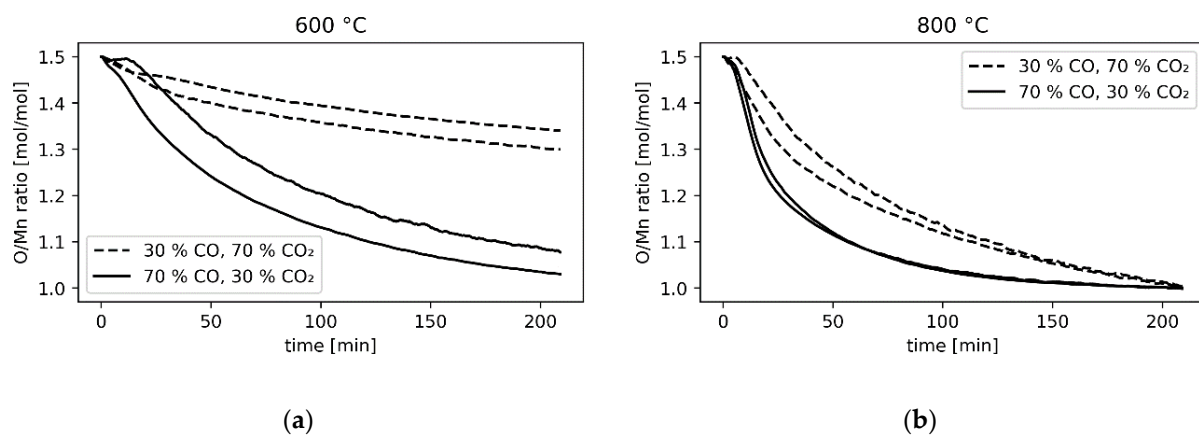


**Figure 6.** The effect of gas composition ( $p_{O_2}$ ) on reduction curves at (a) 600 °C, and (b) 800 °C for the experiments in CO/CO<sub>2</sub> gas mixtures.

The possible sources of weight loss during the experiments were due to a reduction of manganese and iron oxides, in addition to decomposition of carbonates and manganite. Although there is a low content of carbonates in the ore ( $2.5\% \pm 0.5\% \text{ CO}_2$ ), it accounts for a disproportional part of the weight loss if all CO<sub>2</sub> is removed; thus, insight into the decomposition during the experiments is necessary to properly describe the reduction of oxides. The carbonate content of Nchwani ore samples has been reported in the range

0.82–4.8% [12,16,28]. Manganite in the range 1–8% has been reported, implying a weight loss of 0.1–0.82% by H<sub>2</sub>O by decomposition [12,16].

In the hydrogen-containing gas mixtures, all experiments at 700 °C and 800 °C were fully reduced after 210 min (O/Mn = 1.00–1.01 by chemical analyses), and the reduction rate increased with decreasing pO<sub>2</sub>, which is consistent with previous results [15]. Addition of hydrogen was seen to increase the reduction rate less for the low pO<sub>2</sub> parallels (Figure 7a) compared to the high pO<sub>2</sub> parallels (Figure 7b). The use of hydrogen is expected to increase the reduction rate due to its improvement of the diffusion characteristics of the gas mixture. Kononov et al. observed that the carbothermal reduction of MnO proceeded at a higher rate in helium compared to argon due to the increased diffusion coefficients of CO and CO<sub>2</sub> in helium. The rate was further improved when hydrogen was present due to its involvement in the reduction process [29].

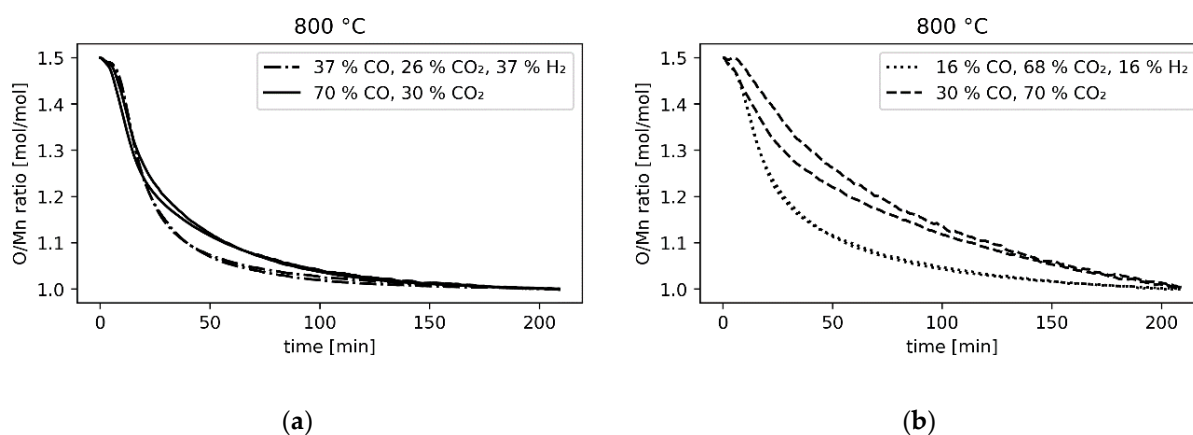


**Figure 7.** The effect of hydrogen at constant oxygen partial pressure at 800 °C for (a) low pO<sub>2</sub>, and (b) high pO<sub>2</sub>.

### 3.1. Modeling

In order to quantify the contributions from changing the oxygen partial pressures and from the addition of hydrogen, modeling was done using a nonlinear least squares method.

$$\frac{d\alpha}{dt} = k(T)f(\alpha) = k_0 \exp\left(-\frac{E_a}{RT(t)}\right)(1-\alpha)^x. \quad (6)$$

Generally, the reduction rate can be described by Equation (6), where the temperature dependency,  $k(T)$ , is parameterized through the Arrhenius equation, and the dependency on the extent of reduction is parameterized through the reaction model,  $f(\alpha)$  [30]. The reaction order model was used, yielding the model expression shown on the right-hand side of Equation (6).

$$\alpha = \frac{\frac{O}{Mn}(t=0) - \frac{O}{Mn}(t)}{\frac{O}{Mn}(t=0) - \frac{O}{Mn}(t=\infty)} = 3 - 2\frac{O}{Mn}(t). \quad (7)$$

The degree of conversion,  $\alpha$ , is defined on the basis of the initial ( $t=0$ ) and final ( $t=\infty$ ) O/Mn ratios according to the chemical analysis and can be seen in Equation (7).

$$\frac{d\alpha}{dt} = \frac{d\alpha}{d\left(\frac{O}{Mn}\right)} \cdot \frac{d\left(\frac{O}{Mn}\right)}{dt} = -2 \frac{d\left(\frac{O}{Mn}\right)}{dt}. \quad (8)$$



According to the chain rule and differentiation of Equation (7), Equation (8) describes the relationship between the rate expressed by  $\alpha$  and the  $O/Mn$  ratio. Insertion of Equations (7) and (8) into Equation (6) yields

$$\frac{d\left(\frac{O}{Mn}\right)}{dt} = -\frac{k_0}{2} \exp\left(-\frac{E_a}{RT(t)}\right) \left(-2\left(1 - \frac{O}{Mn}(t)\right)\right)^x. \quad (9)$$

The reduction rates calculated from the conversion curves in Figure 5 are shown in Figure 8. The reduction rate from each gas mixture was fitted to Equation (9), where  $O/Mn(t)$  is the oxygen manganese molar ratio throughout the experiment,  $d(O/Mn)/dt$  (1/min) is the reduction rate,  $k_0$  (1/min) is the apparent rate constant,  $E_a$  (J/mol) is the apparent activation energy,  $R$  (J/mol·K) is the universal gas constant,  $T(t)$  (K) is the measured temperature as a function of time, and  $x$  is the reaction order.

**Table 5.** The apparent preexponential constant from the modeling with  $E_a = 61$  kJ/mol and  $x = 1.5$ .

Gas Mixture	$k_0$ (1/min)
30% CO—70% CO <sub>2</sub> —0% H <sub>2</sub>	17.7
70% CO—30% CO <sub>2</sub> —0% H <sub>2</sub>	49.2
16% CO—68% CO <sub>2</sub> —16% H <sub>2</sub>	45.2
37% CO—26% CO <sub>2</sub> —37% H <sub>2</sub>	62.1

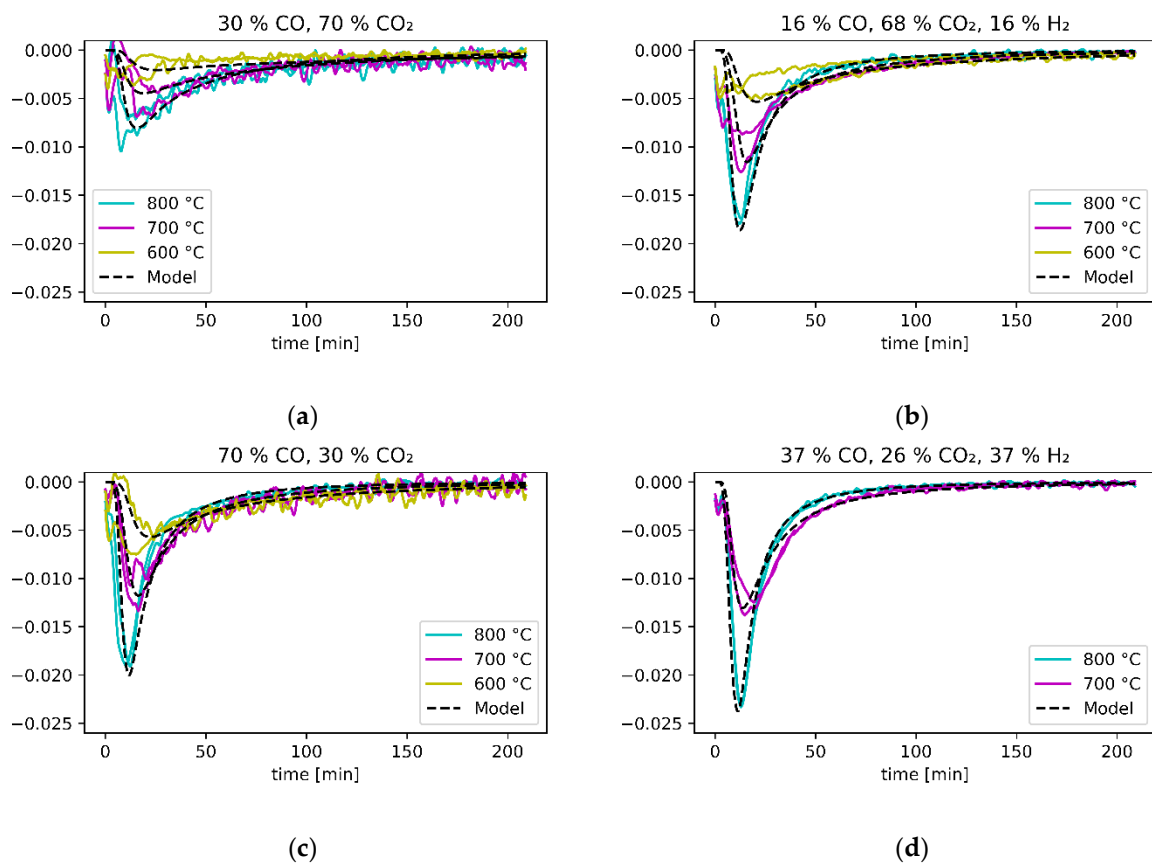


**Figure 8.** The reduction rate as a function of time for the four gas mixtures. The modeling results were superimposed using Equation (9) with  $E_a = 61$ ,  $x = 1.5$ , and  $k_0$  from Table 5. (a): high  $pO_2$  hydrogen-free experiments; (b): high  $pO_2$  hydrogen-containing experiments; (c): low  $pO_2$  hydrogen-free experiments; (d): low  $pO_2$  hydrogen-containing experiments.

An average activation energy from the four parallels of 61 kJ/mol and a reaction order close to 1.5 were found from the model fitting.  $k_0$  was determined on the basis

of these values and can be seen in Table 5. Using this approach, the  $k_0$  values could be compared directly to assess the relative differences between the parallels. The reduction behavior from Equation (9) was calculated using the temperature measurements from the experiments and was superimposed on Figure 8.

The fastest reduction was obtained in the hydrogen-containing low- $pO_2$  gas mixture, whereas the slowest was obtained in the high- $pO_2$  CO–CO<sub>2</sub> mixture. In the CO–CO<sub>2</sub> gas mixtures, increasing the CO content from 30% to 70% increased the reduction rate by a factor of 2.8. The model derived from non-isothermal experiments in Larssen et al. [17] predicted a 3.6-fold increase in the reduction rate by increasing the CO content from 30% to 70%, which is close to the values found in this work. The equivalent change in the hydrogen-containing parallels caused a reduction rate increase by a factor 1.4. The high- $pO_2$  hydrogen-containing and the low- $pO_2$  hydrogen-free gas mixtures were quite similar; in fact, the respective change only increased the reduction rate by 9%, despite it significantly increasing the driving force. The addition of hydrogen increased the reduction rate by factors of 1.3 and 2.6 for the low- and high- $pO_2$  gas mixtures, respectively. In the experiments, hydrogen was added without changing the thermodynamic driving force; hence, the improved reduction rate was a result of improved diffusion characteristics of the reducing gas.

### 3.2. Phase Evolution

The XRD results of the samples reduced at 600 °C in the 30% CO/70% CO<sub>2</sub> atmosphere are shown in Figure 9. After 30 min at 600 °C, the intensity of the bixbyite/braunite peaks increased despite chemical analysis showing a slight reduction in oxygen content ( $O/Mn$ : 1.50 > 1.45). This may be explained by the decomposition of manganite, which is known to decompose to Mn<sub>2</sub>O<sub>3</sub> at this temperature [31]. Hematite, hausmannite, and calcite were still present, and the formation of the monoxide phase (MnO–FeO solid solution) commenced. After 90 min, magnetite was identified in the diffraction pattern, and the increased monoxide content was consistent with the lower  $O/Mn$  ratio in the chemical analysis. When reduction proceeded for 210 min, magnetite and hausmannite could no longer be seen in the XRD spectrum, although the average composition from the chemical analysis indicated a composition close to Mn<sub>3</sub>O<sub>4</sub>. This implies that the original content of hausmannite was reduced; furthermore, if it was formed as an intermediary of the reduction of bixbyite/braunite, its reduction to MnO was fast. This was also seen in Larsen et al., where no hausmannite or magnetite was detected in partly reduced samples (isothermally 50/50 CO/CO<sub>2</sub>; non-isothermally 11.2–15 mm, ~800 °C), indicating that the reduction of hausmannite to manganosite is fast and that the reduction from Mn<sub>2</sub>O<sub>3</sub> to MnO can be considered a single-step reaction [16].

After 30 min reduction at 700 °C in 30% CO/70% CO<sub>2</sub>, the XRD pattern and the  $O/Mn$  ratio were similar to the samples reduced for 210 min at 600 °C. There was less oxygen left in the samples reduced at 800 °C compared to 600 °C and 700 °C. The XRD shows that some Mn<sub>2</sub>O<sub>3</sub> (bixbyite/braunite) was still present in the fully reduced ( $O/Mn$  = 1.00–1.01) samples. Magnetite was identified after 90 min reduction at 700 °C, but no iron-containing phases were identified after 210 min reduction. The higher oxides of iron may have been dissolved in the bixbyite phase or reduced to FeO and dissolved in the MnO phase. The experiments reduced for 210 min at 700 °C obtained  $O/Mn$  ratios of 1.18 and 1.00. A significant difference in the chemical analysis between the two parallels was their Mn/Fe ratio which were 2.4 and 8.9 compared to 5.6 for the unreduced ore.

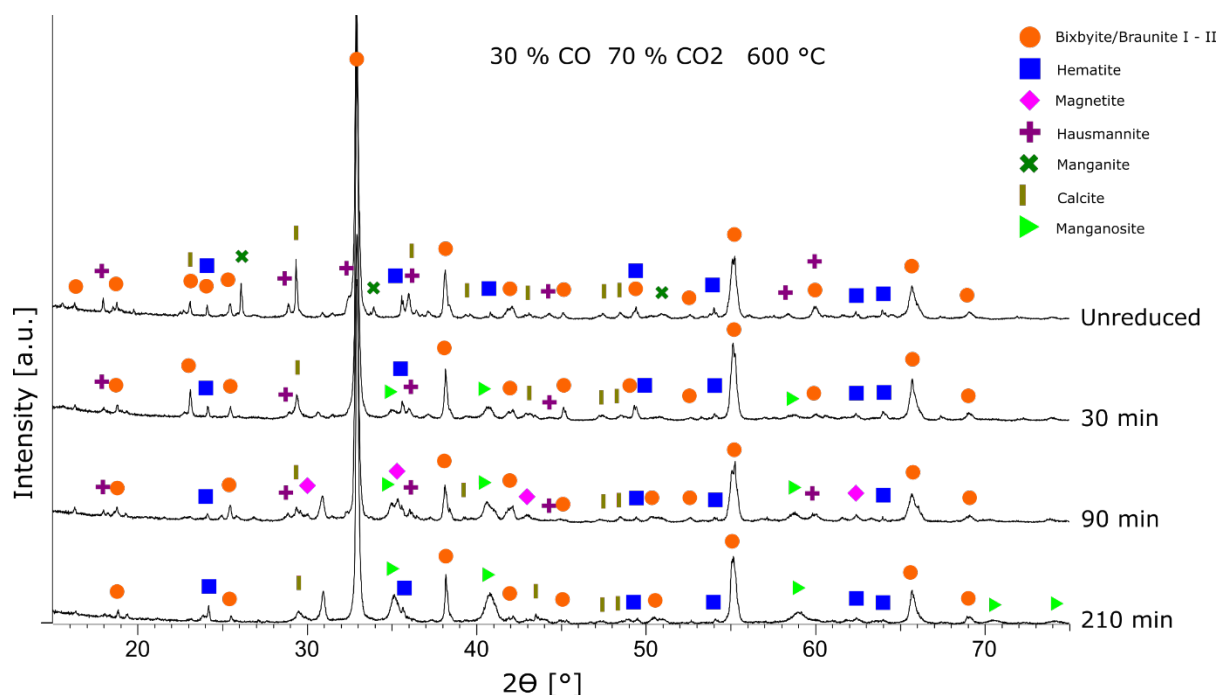


**Figure 9.** X-ray diffraction patterns and identified phases in unreduced ore and samples reduced in 30% CO and 70% CO<sub>2</sub> at 600 °C. The main bixbyite/braunite peak (33°) is cropped for clarity in the figure.

Magnetite was identified after 210 min at 800 °C and 30% CO/70% CO<sub>2</sub> in the fully reduced sample with the highest iron content (13.5% Fe). From Figure 4, it can be seen that MnO–FeO displayed complete solid solubility, and that more than 50 mol.% of the cations may be Fe in the bixbyite phase at 800 °C; on the other hand, less than 10 mol.% of the cations may be Fe in hausmannite. The magnetite in the most reduced sample may have been expelled from the bixbyite upon reduction and was still present due to its higher stability compared to hausmannite (Figure 3).

Samples reduced in 70% CO and 30% CO<sub>2</sub> had a lower *O/Mn* ratio compared to their 30% CO counterparts, as also seen in the reduction curves (Figure 5). At 600 °C, the bixbyite/braunite and hematite content decreased as time progressed. Hematite was identified up until 90 min, whereas, at 210 min, magnetite was identified. The 90 min and 210 min samples had a relatively high iron content (11.5% and 12.8% Fe, respectively). At 700 °C, hausmannite disappeared after 90 min, whereas hematite was still present at 210 min, parallel with the highest iron content (14.5 wt.%). At 800 °C, there was no hausmannite in the samples reduced for 30 min. After 90 and 210 min, tephroite was observed, while hematite and magnetite were not present.

Figures 10 and 11 shows the XRD spectra for the samples reduced in 16% CO/68% CO<sub>2</sub>/16% H<sub>2</sub> and 37% CO/26% CO<sub>2</sub>/37% H<sub>2</sub>, respectively. The amount of bixbyite/braunite decreased and the monoxide increased with increasing temperature for both gas mixtures. Tephroite was found when the ore was reduced at 800 °C for both gas mixtures. At 700 °C and 800 °C, the samples were fully reduced according to the chemical analysis (*O/Mn* = 1.00–1.01), although there were traces of Mn<sub>2</sub>O<sub>3</sub>. No hematite or magnetite was identified in any of the samples reduced with H<sub>2</sub> present in the gas.

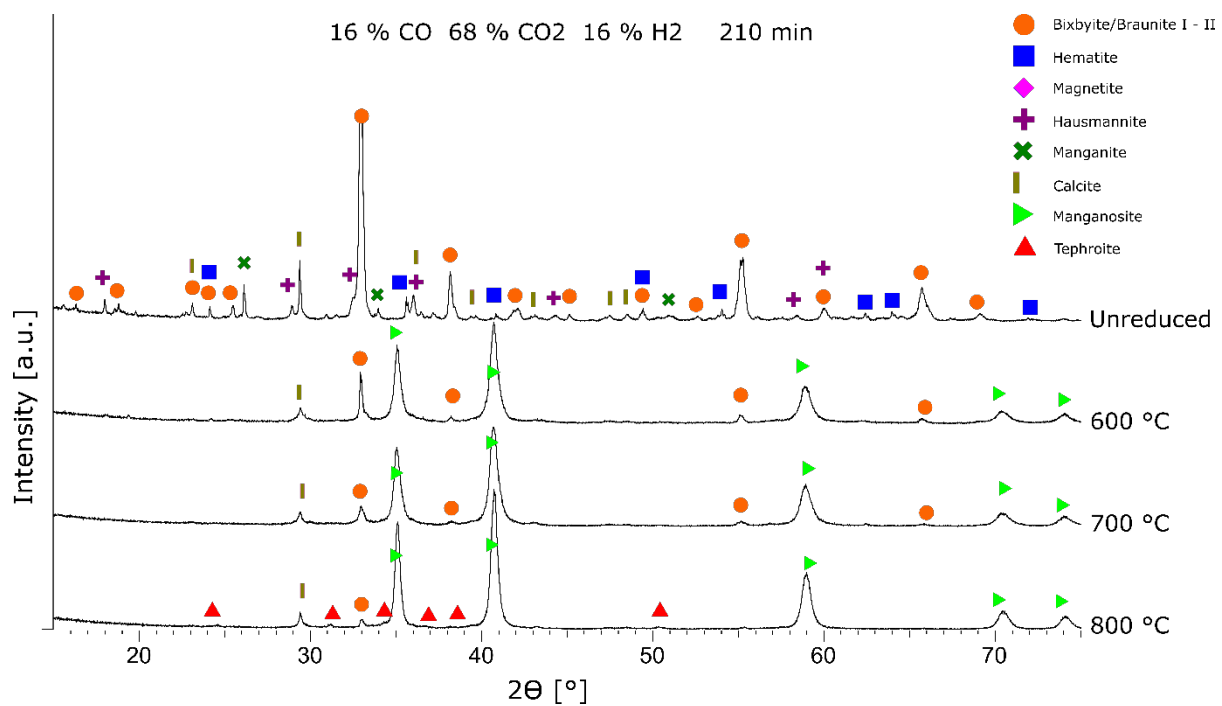


Figure 10. X-ray diffraction patterns from the experiments conducted with the 16% CO/68 CO<sub>2</sub>/16% H<sub>2</sub> gas mixture.

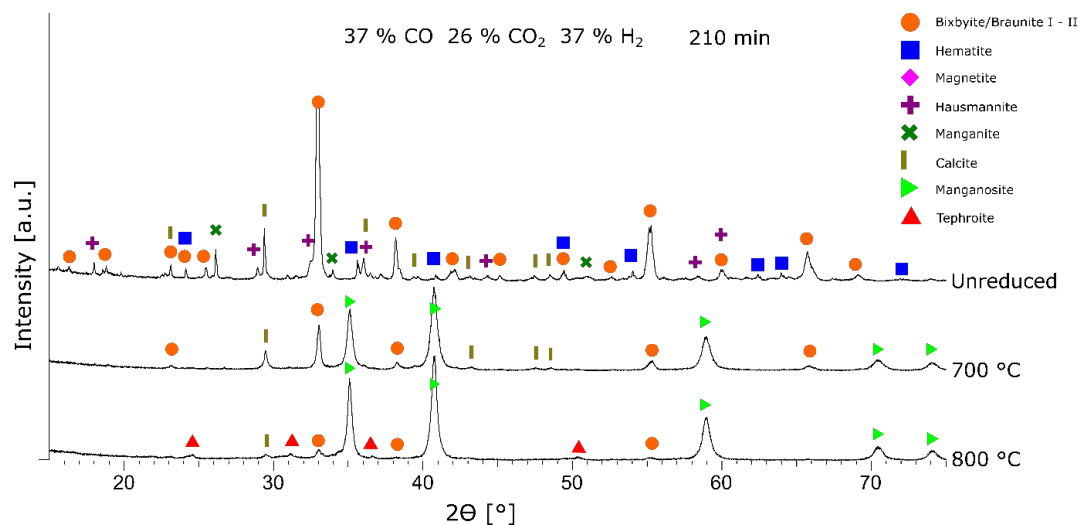
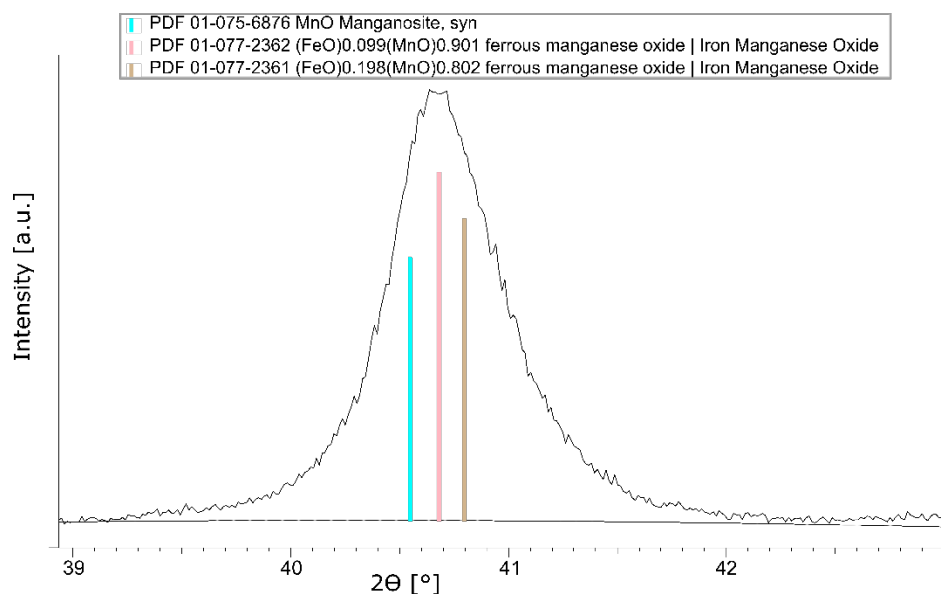


Figure 11. X-ray diffraction patterns from the experiments conducted with the 37% CO/26 CO<sub>2</sub>/37% H<sub>2</sub> gas mixture.

In general, from the XRD analysis, it can be seen that bixbyite/braunite was reduced, and monoxide was produced. The monoxide phase also dissolved iron, as seen in Figure 12. The relative minor presence of hausmannite in the partly reduced samples may have been due to either the original content in the unreduced ore or to an intermediary that was quickly reduced. There were several samples where bixbyite/braunite and monoxide were present, without indications of hausmannite. From studies of synthetic manganese oxides, stepwise reduction was only observed in oxidizing and inert atmospheres, whereas, in reducing atmospheres, MnO<sub>2</sub> reduced to MnO without the formation of stable intermediaries [32]. Samples with high iron content often retained hematite or magnetite when reduced in CO/CO<sub>2</sub>, but not when hydrogen was used. This indicates that the presence of hydrogen improves the reduction of iron oxides, as previously observed in the reduction of iron ores [33–35]. In all cases where parallel experiments were analyzed, the sample with the higher iron content had a lower or equal O/Mn ratio; hence, high iron content seems

to favor the reduction of manganese oxides. This may be via dilution or absorption/solid solution since both hematite and magnetite may dissolve and stabilize the corresponding manganese oxides (Figure 4). Formation of tephroite was seen in many of the samples reduced at 800 °C. Manganese in tephroite had the same oxidation state as manganese in manganosite; hence, the formation of tephroite had no impact on the prereduction. Bixbyite/braunite was still present in many of the samples where chemical analysis stated that they were fully reduced ( $O/Mn = 1$ ). As mentioned previously, bixbyite may dissolve a significant amount of iron and may be saturated with iron if the manganese is reduced first, but it will still consist of more than 40% Mn cations. This implies that the oxygen measurement in the chemical analysis underestimated the oxygen content of the sample, and that it may have been caused by a high amount of iron in the bixbyite phase. Carbonates were present in all XRD patterns with lower peak intensity compared to the unreduced material.



**Figure 12.** Main peak from the monoxide phase of one of the samples reduced for 210 min in 70% CO–30% CO<sub>2</sub> at 700 °C.

### 3.3. Carbonate Decomposition

Carbonates are often present in the ore and decompose to release CO<sub>2</sub>. The carbonates of calcium, magnesium and manganese, as well as dolomite (CaMg(CO<sub>3</sub>)<sub>2</sub>) and kutnohorite (CaMn(CO<sub>3</sub>)<sub>2</sub>), are found in manganese ores [12,36–39]. Calcite has the highest decomposition temperature of the carbonates of 892 °C ( $p_{CO_2} = 1$ ) and will contribute with CO<sub>2</sub> to the Boudouard reaction. The other carbonates may decompose at temperatures below 800 °C [40,41]. Figure 13 shows the stability of selected carbonates as a function of temperature and CO<sub>2</sub> partial pressure, where the CO<sub>2</sub> content of the utilized gas mixtures is indicated. It can be seen that calcite was stable under the current experimental conditions and that dolomite, in addition to magnesium and manganese carbonate, could decompose.

According to the chemical reactions for decomposition of carbonates (i.e., reaction (10)), any carbonates present in the ore are stabilized by CO<sub>2</sub>.



Carbonate decomposition is known to depend on temperature and CO<sub>2</sub> content in the atmosphere [42,43]; this has also been seen in the case of manganese ores [27]. The remaining content of CO<sub>2</sub> in the samples was analyzed after reduction. Figure 14 shows the remaining carbonates as a function of the CO<sub>2</sub> content of the reducing atmosphere after 210 min. The slopes of the lines were calculated from the linear regression of all points, while the  $y$ -intercepts were calculated from fitting at each temperature. It can be seen that,

for decreasing temperature and for increasing CO<sub>2</sub> content of the reducing atmosphere, more carbonates remained in the sample after reduction for 210 min. According to the differences in the lines in Figure 14, on average, the samples lost 1.3 wt.% more mass from carbonates when increasing the temperature from 600 °C to 700 °C and 0.4 wt.% more mass when increasing the temperature from 700 °C to 800 °C. Despite these differences, only a small proportion of carbonates were removed during reduction in the current experimental conditions. Larssen et al. found magnesium and manganese in addition to calcium in the carbonate phase of Nchwanging ore [16], which explains the relatively minor removal of carbonates. Calcite was stable under the experimental conditions, whereas the carbonates of magnesium and manganese were not.

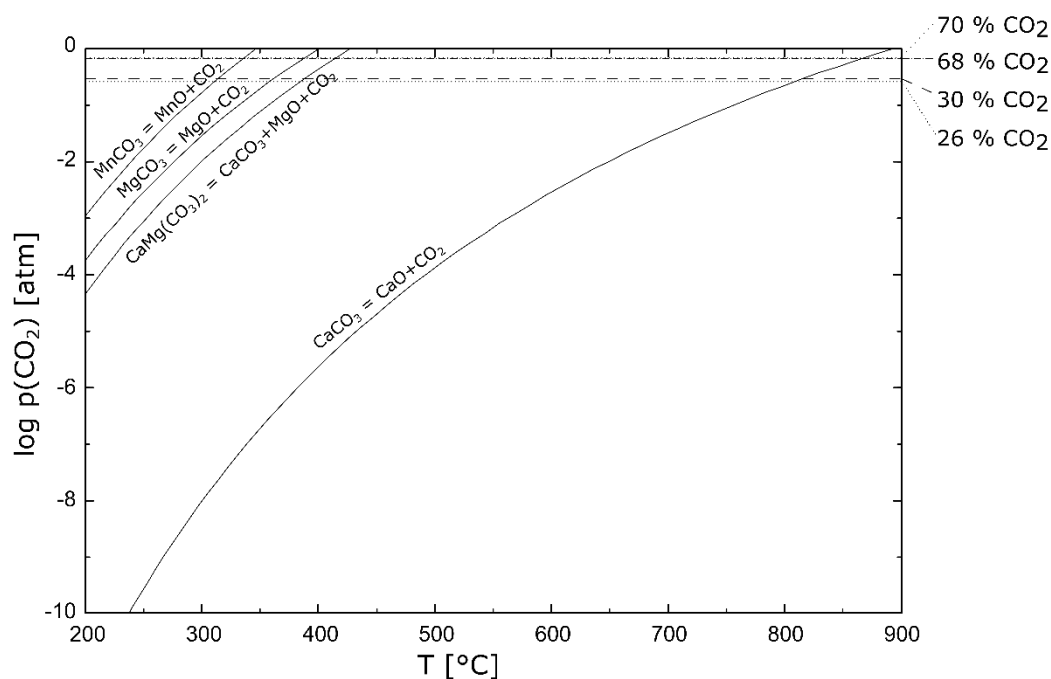


Figure 13. The stability of selected carbonates as a function of carbon dioxide partial pressure and temperature. The CO<sub>2</sub> content of the utilized gas mixtures is indicated in the figure.

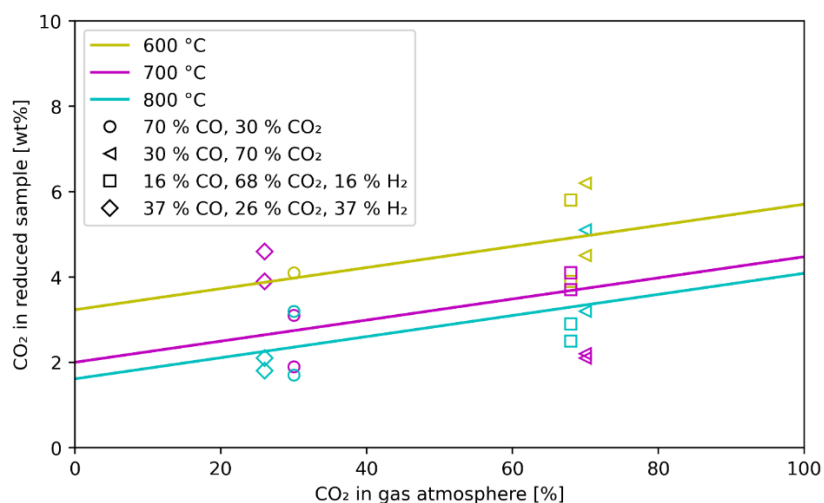


Figure 14. Analyzed CO<sub>2</sub> in the reduced sample as a function of the CO<sub>2</sub> in the reducing atmosphere. Linear regression of all points gave the slope, which led to the colored lines fitting to the different temperatures. Only the 210 min experiments are included.



#### 4. Conclusions

The reduction of Nchwanning manganese ore was investigated at two different oxygen partial pressures using gas CO/CO<sub>2</sub> gas mixtures with and without H<sub>2</sub>. The reduction rate was seen to increase with increasing temperature and with decreasing oxygen partial pressure. Addition of hydrogen at constant oxygen partial pressure increased the reduction rate. The reduction behavior was quantified by modeling, and it was found that increasing the CO content from 30% to 70% in a CO/CO<sub>2</sub> gas mixture increased the reduction rate by a factor of 2.8. Replacing parts of the CO with hydrogen in the gas mixtures increased the reduction rate 1.3–2.6-fold when the oxygen partial pressure was kept constant. To achieve an optimal pretreatment, the temperature of the pretreatment unit must be high while keeping the oxygen partial pressure low and adding hydrogen to the reducing gas. If the highest degree of reduction attained in this work is achieved industrially, savings in the range of 51–81 kg of C and 202–354 kWh electric energy per ton of metal produced can be realized.

The results from XRD analysis are consistent with the reduction behavior. It was seen that hausmannite initially present in the ore was quickly reduced, and bixbyite/braunite was reduced to manganosite without the formation of stable hausmannite as an intermediary phase. Iron oxides were reduced more slowly than manganese oxides, and the reduction subsided with wüstite as it was stabilized in solid solution with manganosite. The presence of hydrogen was seen to improve the reduction of iron oxides.

A fraction of the carbonates, associated with manganese and magnesium, decomposed under the current conditions. Decomposition was promoted by higher temperature and lower CO<sub>2</sub> content in the reducing gas.

If a pretreatment unit runs on furnace off-gas in the temperature range studied in this work, it may prereducer the manganese and iron oxides to monoxide prior to charging in the furnace. Improving prereducer limits the extent of the Boudouard reaction, causing the furnace gas to contain less CO. The addition of hydrogen gas to the pretreatment unit may compensate for the increased oxygen partial pressure in addition to further improving the kinetics of reduction.

**Author Contributions:** Experiments, data analysis, and original draft preparation, T.L.S.; review and editing, M.T. All authors have read and agreed to the published version of the manuscript.

**Funding:** The authors gratefully acknowledge the financial support from the Research Council of Norway (Grant number: 280968) and our industrial partners Elkem ASA, TiZir Titanium & Iron AS, Eramet Norway AS, Finnjord AS, and Wacker Chemicals Norway AS for financing the “KPN reduced CO<sub>2</sub> emissions in metal production” project.

**Data Availability Statement:** Data is contained within the article.

**Conflicts of Interest:** The authors declare no conflict of interest. The funders had no role in the design of the study; in the collection, analyses, or interpretation of data; in the writing of the manuscript, or in the decision to publish the results.

#### References

1. Olsen, S.E.; Tangstad, M.; Lindstad, T. *Production of Manganese Ferroalloys*; Tapir ACADEMIC Press: Trondheim, Norway, 2007; ISBN 978-82-519-2191-6.
2. Ishak, R.; Tangstad, M. Degree of Prereducer Without Coke Consumption in Industrial Furnaces. In Proceedings of the XI International Conference on Innovations in the Ferro Alloy Industry, New Delhi, India, 18–21 February 2007.
3. Tangstad, M.; Ichihara, K.; Ringdalen, E. Pretreatment Unit in Ferromanganese Production. In Proceedings of the The Fourteenth International Ferroalloys Congress, Kiev, Ukraine, 31 May–4 June 2015.
4. Schanche, T.L.; Tangstad, M. Isothermal Reduction of Nchwanning Manganese Ore in CO/CO<sub>2</sub>/H<sub>2</sub> Atmospheres. In Proceedings of the 16th International Ferro-Alloys Congress, Trondheim, Norway, 27–29 September 2021.
5. Ishitobi, T.; Ichihara, K.; Homma, T. Operational Improvements of a Submerged Arc Furnace in Kashima Works (kf-1) Relined in 2006. In Proceedings of the Twelfth International Ferroalloys Congress, Helsinki, Finland, 6–9 June 2010.
6. Yoshida, F.; Honma, T.; Sasaki, T. Automation and Reduction of Labor in the Operation of Electric Arc Furnace for HCFMn Production. In Proceedings of the 8th International Ferro-Alloys Congress, Beijing, China, 7–10 June 1998.

7. Teguri, D.; Saito, K.; Miyauchi, Y. Manganese Ore Pre-Reduction Using a Rotary Kiln to Manufacture Super-Low-Phosphorus Ferromanganese. In Proceedings of the Infacon XV International Ferro-Alloys Congress, Cape Town, South Africa, 25–28 February 2018.
8. Swamy, K.N.; Robertson, D.G.C.; Calvert, P.; Kozak, D. Factors Affecting Carbon Consumption in the Production of High Carbon Ferromanganese. In Proceedings of the 9th International Ferro-Alloys Congress, Quebec City, QC, Canada, 3–6 June 2001.
9. Pochart, G.; Joncourt, L.; Touchard, N.; Perdon, C. Metallurgical Benefit of Reactive High Grade Ore in Manganese Alloys Manufacturing. In Proceedings of the 11th International Ferro-Alloys Congress, New Delhi, India, 18–21 February 2007.
10. Soller, A.; Amalric, A.; Pochart, G.; Nussbaum, G. Manganese Ore and Alloys Piloting Tools at Eramet Research. In Proceedings of the 12th International Ferro-Alloys Congress, Helsinki, Finland, 6–9 June 2010.
11. Tangstad, M.; Leroy, D.; Ringdalen, E. Behavior of Agglomerates in Ferromanganese Production. In Proceedings of the 12th International Ferro-Alloys Congress, Helsinki, Finland, 6–9 June 2010.
12. Visser, M.; Smith, H.; Ringdalen, E.; Tangstad, M. PROPERTIES OF NCHWANINGAND GLORIA ORE IN THE PRODUCTION OF Mn FERRO-ALLOYS. In Proceedings of the 13th International Ferro-Alloys Congress, Almaty, Kazakhstan, 9–13 June 2013.
13. Turkova, K.; Slizovskiy, D.; Tangstad, M. CO Reactivity and Porosity of Manganese Materials. *ISIJ Int.* **2014**, *54*, 1204–1208. [[CrossRef](#)]
14. Jesus, L.G.M.D.; Tangstad, M. CO Reactivity of Manganese Lumps Versus Briquettes. *ISIJ Int.* **2020**, *60*, 2129–2133. [[CrossRef](#)]
15. Ngoy, D.; Sukhomlinov, D.; Tangstad, M. Pre-Reduction Behaviour of Manganese Ores in H<sub>2</sub> and CO Containing Gases. *ISIJ Int.* **2020**, *60*, 7. [[CrossRef](#)]
16. Larssen, T.A.; Senk, D.; Tangstad, M. Reduction of Manganese Ores in CO-CO<sub>2</sub> Atmospheres. *Metall. Mater. Trans. B* **2020**, *52*, 363–381. [[CrossRef](#)]
17. Larssen, T.A.; Senk, D.; Tangstad, M. Reaction Rate Analysis of Manganese Ore Prereduction in CO-CO<sub>2</sub> Atmosphere. *Metall. Mater. Trans. B* **2021**, *52*, 2087–2100. [[CrossRef](#)]
18. Szekely, J.; Evans, J.W.; Sohn, H.Y. *Gas-Solid Reactions*; Academic Press: New York, NY, USA, 1976; ISBN 0-12-680850-3.
19. Eissa, M.; El-Faramawy, H.; Ahmed, A.; Nabil, S.; Halfa, H. Parameters Affecting the Production of High Carbon Ferromanganese in Closed Submerged Arc Furnace. *J. Miner. Mater. Charact. Eng.* **2012**, *11*, 1–20. [[CrossRef](#)]
20. Ahmed, A.; Haifa, H.; El-Fawakhry, M.K.; El-Faramawy, H.; Eissa, M. Parameters Affecting Energy Consumption for Producing High Carbon Ferromanganese in a Closed Submerged Arc Furnace. *J. Iron Steel Res. Int.* **2014**, *21*, 666–672. [[CrossRef](#)]
21. Bale, C.W.; Bélisle, E.; Chartrand, P.; Decterov, S.A.; Eriksson, G.; Gheribi, A.E.; Hack, K.; Jung, I.-H.; Kang, Y.-B.; Melançon, J.; et al. FactSage Thermochemical Software and Databases, 2010–2016. *Calphad* **2016**, *54*, 35–53. [[CrossRef](#)]
22. Roine, A. *HSC Chemistry*<sup>®</sup>; Outotec: Pori, Finland, 2018.
23. Villiers, J.P.R.D. The Crystal Structure of Braunitz II and Its Relation to Bixbyite and Braunitz. *Am. Mineral.* **1980**, *65*, 756–765.
24. Berg, K.L.; Olsen, S.E. Kinetics of Manganese Ore Reduction by Carbon Monoxide. *Metall. Mater. Trans. B* **2000**, *31*, 477–490. [[CrossRef](#)]
25. Gao, Y.B.; Kim, H.G.; Sohn, H.Y. Kinetics of Pre-Reduction of Manganese Ore by CO. *Miner. Process. Extr. Metall. Trans. Inst. Min. Metall. Sect. C* **2012**, *121*, 109–116. [[CrossRef](#)]
26. Fahim, M.S.; El Faramawy, H.; Ahmed, A.M.; Ghali, S.N.; Kandil, A.E.H.T. Characterization of Egyptian Manganese Ores for Production of High Carbon Ferromanganese. *J. Miner. Mater. Charact. Eng.* **2013**, *1*, 68–74. [[CrossRef](#)]
27. Sukhomlinov, D.; Tangstad, M. Non-Isothermal Pre-Reduction of Carbonated Manganese Ore by Carbon Monoxide. Metals To be published.
28. Ngoy, D.M.; Tangstad, M.; Kalenga, M. Reduction Rate of MnO from Two Different Manganese Ores Producing Ferromanganese. In Proceedings of the Infacon XV International Ferro-Alloys Congress, Cape Town, South Africa, 25–28 February 2018.
29. Kononov, R.; Ostrovski, O.; Ganguly, S. Carbothermal Reduction of Manganese Oxide in Different Gas Atmospheres. *Metall. Mater. Trans. B* **2008**, *39*, 662–668. [[CrossRef](#)]
30. Vyazovkin, S.; Burnham, A.K.; Criado, J.M.; Pérez-Maqueda, L.A.; Popescu, C.; Sbirrazzuoli, N. ICTAC Kinetics Committee Recommendations for Performing Kinetic Computations on Thermal Analysis Data. *Thermochim. Acta* **2011**, *520*, 1–19. [[CrossRef](#)]
31. Morgan, D.J.; Milodowski, A.E.; St J Warne, S.; Warrington, S. Atmosphere Dependence of the Thermal Decomposition of Manganite,  $\gamma$ -MnO.OH. *Thermochim. Acta* **1988**, *135*, 273–277. [[CrossRef](#)]
32. Zaki, M.I.; Hasan, M.A.; Pasupulety, L.; Kumari, K. Thermochemistry of Manganese Oxides in Reactive Gas Atmospheres: Probing Redox Compositions in the Decomposition Course  $\text{MnO}_2 \rightarrow \text{MnO}$ . *Thermochim. Acta* **1997**, *303*, 171–181. [[CrossRef](#)]
33. Piotrowski, K.; Mondal, K.; Lorethova, H.; Stonawski, L.; Szymański, T.; Wiltowski, T. Effect of Gas Composition on the Kinetics of Iron Oxide Reduction in a Hydrogen Production Process. *Int. J. Hydrog. Energy* **2005**, *30*, 1543–1554. [[CrossRef](#)]
34. Pineau, A.; Kanari, N.; Gaballah, I. Kinetics of Reduction of Iron Oxides by H<sub>2</sub>: Part I: Low Temperature Reduction of Hematite. *Thermochim. Acta* **2006**, *447*, 89–100. [[CrossRef](#)]
35. Pineau, A.; Kanari, N.; Gaballah, I. Kinetics of Reduction of Iron Oxides by H<sub>2</sub>: Part II. Low Temperature Reduction of Magnetite. *Thermochim. Acta* **2007**, *456*, 75–88. [[CrossRef](#)]
36. Coetsee, T. The Role of Manganese Ore Reduction Morphology Development in Setting Reduction Mechanisms. *Miner. Eng.* **2019**, *137*, 217–231. [[CrossRef](#)]
37. Faria, G.L.; Jannotti, N.; da Silva Araújo, F.G. Decrepitation Behavior of Manganese Lump Ores. *Int. J. Miner. Process.* **2012**, *102–103*, 150–155. [[CrossRef](#)]

38. O'Shaughnessy, P.; Kon, K.J.; Wha, L.B. The Smelting of Manganese Carbonate Ore. In Proceedings of the 10th International Ferro-Alloys Congress, Cape Town, South Africa, 1–4 February 2004.
39. Pereira, M.J.; Lima, M.M.F.; Lima, R.M.F. Calcination and Characterisation Studies of a Brazilian Manganese Ore Tailing. *Int. J. Miner. Process.* **2014**, *131*, 26–30. [[CrossRef](#)]
40. Engler, P.; Santana, M.W.; Mittleman, M.L.; Balazs, D. Non-Isothermal, in Situ XRD Analysis of Dolomite Decomposition. *Thermochim. Acta* **1989**, *140*, 67–76. [[CrossRef](#)]
41. Iwafuchi, K.; Watanabe, C.; Otsuka, R. Thermal Decomposition of Magnesian Kutnahorite. *Thermochim. Acta* **1983**, *60*, 361–381. [[CrossRef](#)]
42. Criado, J.M.; Gonzalez, F.; Gonzalez, M. Influence of the CO<sub>2</sub> Pressure on the Kinetics of Thermal Decomposition of Manganese Carbonate. *J. Therm. Anal.* **1982**, *24*, 59–65. [[CrossRef](#)]
43. Wang, Y.; Lin, S.; Suzuki, Y. Study of Limestone Calcination with CO<sub>2</sub> Capture: Decomposition Behavior in a CO<sub>2</sub> Atmosphere. *Energy Fuels* **2007**, *21*, 3317–3321. [[CrossRef](#)]